

Vortex lattice dynamics in Nb films with competing intrinsic random and artificial periodic pinning

This article has been downloaded from IOPscience. Please scroll down to see the full text article.

2011 Supercond. Sci. Technol. 24 065008

(<http://iopscience.iop.org/0953-2048/24/6/065008>)

View [the table of contents for this issue](#), or go to the [journal homepage](#) for more

Download details:

IP Address: 132.239.69.137

The article was downloaded on 20/10/2011 at 00:39

Please note that [terms and conditions apply](#).

Vortex lattice dynamics in Nb films with competing intrinsic random and artificial periodic pinning

C Chilotte¹, G Pasquini¹, V Bekeris¹, J E Villegas^{2,3}, C-P Li⁴ and Ivan K Schuller⁴

¹ Departamento de Física, FCEyN, Universidad de Buenos Aires and IFIBA, CONICET, Pabellón 1, Ciudad Universitaria, Buenos Aires, Argentina

² Unité Mixte de Physique CNRS/Thales, 1 avenue A Fresnel, 91767 Palaiseau, France

³ Université Paris Sud 11, 91405 Orsay, France

⁴ Physics Department, University of California-San Diego, La Jolla, CA 92093-0319, USA

E-mail: vbekeris@df.uba.ar

Received 25 January 2011, in final form 10 March 2011

Published 1 April 2011

Online at stacks.iop.org/SUST/24/065008

Abstract

We study vortex lattice (VL) dynamics in patterned Nb films containing dense periodic arrays of sub 50 nm magnetic nanodots or holes, by means of ac susceptibility measurements. For both types of samples, we observe matching effects within a wide temperature range, determined by the periodicity of the strong artificial pinning potential. Below a crossover reduced temperature $t^* = 0.75$, the ac vortex mobility and matching fields are different for increasing or decreasing fields. Low temperature field cooling experiments indicate that the hysteretic behavior is not related to different intensities of magnetic induction B in the ac penetrated region of the samples. The fact that hysteresis appears in both patterned samples when the intrinsic random pinning becomes stronger, together with the absence of hysteresis in a reference unpatterned Nb film, suggests that the interplay between random and periodic pinning, independent of its origin, induces VL metastability below t^* , which leads to the observed irreversibility.

(Some figures in this article are in colour only in the electronic version)

1. Introduction

The response of the vortex lattice (VL) in conventional low T_c superconducting films, for which thermal fluctuations are negligible and random quenched disorder leads to moderate VL pinning, has been usually described in terms of the critical state model [1]. In general, intrinsic vortex pinning defects in films are randomly distributed within the sample, and present also a random distribution in intensity. Contrary to this, artificial pinning allows the creation of ordered distributions of pinning sites, all of these having virtually the same intensity, in order to study the interplay between random and ordered pinning. There are a variety of techniques to fabricate artificial arrays of pinning centers with different geometries: periodic [2–6], quasiperiodic [7, 8], fractal [7] or with controlled degrees of disorder [9]. For example, periodic patterns of submicrometric magnetic inclusions [10]

(for an extensive review see [11, 12]) produce distortions in currents and the magnetic field, and these distortions determine the pinning landscape. A different type of periodic pinning mechanism is related to the suppression of the superconducting order parameter, either induced by proximity effects emerging from periodic normal inclusions [13] or by periodic modulation of the sample thickness produced for example by blind holes [14]. Arrays of holes or pores in superconducting films have been shown to be efficient artificial pinning centers [3, 15].

The well known fingerprints of strong periodic pinning centers are matching anomalies, which generally occur for applied fields that produce a number of vortex lines equal to the number of artificial pinning sites [6]. At the so-called first matching field, H_M , the VL matches the geometry of the artificial pinning potential to minimize the system's free energy, and pinning is collectively increased producing a peak

in the critical current density. Integer [16], and in some cases fractional, multiples of the first matching field [17] may also give rise to matching anomalies, according to the symmetry of the periodic potential and to the size of the pinning sites (which determines the maximum number of flux quanta that can be pinned per site).

Regardless of the type of artificial pinning site, quenched disorder in interstitial regions provides random pinning if those regions are large enough to accommodate vortices. When artificial and intrinsic pinning have comparable strength, the competition between both will govern the vortex dynamics [18] giving rise to a distinct hysteretic behavior, as we shall show below.

In particular, as temperature is reduced below the superconducting critical temperature, T_c , the pinning forces from intrinsic defects may overcome the artificial periodic pinning forces. For this reason, matching anomalies are usually observed only at temperatures close to T_c [15, 19]. However, if the interstitial superconducting film has moderate or weak quenched disorder, or if the artificial pinning sites are sufficiently strong, the periodic pinning potential will remain relevant in a wide temperature range below T_c [20], allowing a systematic study of the vortex lattice behavior when artificial periodic and intrinsic random pinning coexist and interplay [21].

In this work we report on ac susceptibility measurements in unpatterned and patterned Nb films containing a triangular array of either sub-50 nm Fe dots or holes. We found matching effects in vortex mobility in a wide temperature range, $0.5 < t < 0.95$, for both patterned samples, where $t = T/T_c$ is the reduced temperature and T_c is the critical temperature of each sample. Below a reduced crossover temperature, $t^* \sim 0.75$, as intrinsic interstitial random pinning increases, we found that matching is accompanied by a characteristic hysteretic behavior that can be consistently described as arising from the coexistence and competition of random and periodic pinning. Moreover, the above effects evidence that matching phenomena in Nb films containing triangular arrays of nano-holes arise from flux pinning, rather than from Little–Parks effects as recently proposed [22] based on the ‘wire network’ structure of this type of sample. In addition to vortex dynamics, these results may be relevant for other physical systems, such as colloids [23] or charge density waves, in which an elastic lattice moves on a pinning landscape [24] where order and disorder coexist and compete.

The paper is organized as follows. In section 2 we describe the samples and the experimental techniques. Section 3 contains the results and the discussion. Conclusions are presented in section 4.

2. Experimental details

Ac susceptibility measurements, $\chi_{ac}(H, T) = \chi'(H, T) + j\chi''(H, T)$, were performed in a commercial QD MPMS XL 7 T magnetometer. This technique allows inspection of the superconductivity in the low temperature/field ranges where transport is no longer useful due to the high critical currents. An applied ac magnetic field modulates the dc field

that creates vortices inside the sample and the complex ac penetration depth related to $\chi_{ac}(H, T)$ and sample geometry is measured using an array of secondary coils [25]. In the nonlinear regime, $\chi_{ac}(H, T)$ is h_{ac} dependent and ac losses are not negligible, vortices make excursions outside the effective pinning wells and a small ac penetration depth or high screening ($\chi'(H, T) \sim -1$), is related to a VL with low mobility. On the contrary, a large ac penetration depth ($\chi'(H, T) \sim 0$) results for a weakly pinned, highly mobile VL.

In all cases, ac susceptibility measurements were made in ac and dc magnetic fields applied perpendicular to the samples. The measurements reported in this work are in the nonlinear regime at audio frequency, $f \sim 1$ kHz, and ac amplitude $h_{ac} = 1$ Oe, indicating that vortices are forced out of their effective pinning potential wells, and that mobility is tested. To determine the critical onset temperature and transition width for each sample, the applied ac field was reduced to $h_{ac} = 0.01$ Oe.

Results for three types of superconducting films are presented in this paper. Sample A is a plain Nb film used as reference, containing only intrinsic pinning defects. Samples B and C are both nanostructured Nb films containing periodic arrays of artificial pinning sites. In the case of sample B, the film contains an array of sub-50 nm magnetic dots, while sample C has an array of sub-50 nm ‘antidots’ or holes.

For sample A a 100 nm thick Nb film was deposited on top of a Si substrate using electron beam evaporation (chamber base pressure 10^{-11} Torr, typical substrate dimensions 2×3 mm²). This reference film has an onset superconducting critical temperature of $T_{co}^A = (8.25 \pm 0.05)$ K, defined as the onset of the ac susceptibility transition at $H = 0$, and a 10%–90% transition width $\Delta T_c = 0.12$ K. Sample B is a 100 nm thick Nb film (2.5×3.5 mm²) deposited using the same technique on a triangular array of 40 nm thick Fe nanodots with diameter $\Phi = 40$ nm. The interdot distance is $d = 100$ nm. The dispersions Δd and $\Delta \Phi$ are less than $\pm 10\%$, as found by statistical analysis of scanning electron microscopy (SEM) images of the dot array (not shown) prior to Nb deposition. The nanodot array was obtained by evaporating Fe through a porous alumina mask, as described elsewhere [26, 27]. Prior to Nb deposition, a 10 nm SiO₂ film was deposited on top of the Fe nanodots in order to electrically isolate the superconducting film from the nanodots, thus preventing proximity effects. In this way, vortex pinning is produced solely by the magnetostatic interaction between vortices and stray fields of the magnetic dots, and by the array-induced corrugation of the Nb film. The superconducting onset as measured by ac susceptibility for sample B is $T_{co}^B = (7.35 \pm 0.05)$ K with the 10%–90% transition width $\Delta T_c = 0.6$ K.

Sample C is a 100 nm thick Nb film (2×3 mm²) directly sputtered on a clean porous alumina mask, similar to the one used to fabricate the Fe nanodot array. This Nb film contains a triangular array of pores, or antidots, separated at $d = 100$ nm with an average pore diameter $\Phi = 40$ nm, as shown in the SEM micrograph in figure 1(a). For this sample we also found Δd and $\Delta \Phi \simeq \pm 10\%$. The porous Nb film has a zero-field critical temperature onset $T_{co}^C = (7.25 \pm 0.05)$ K and the

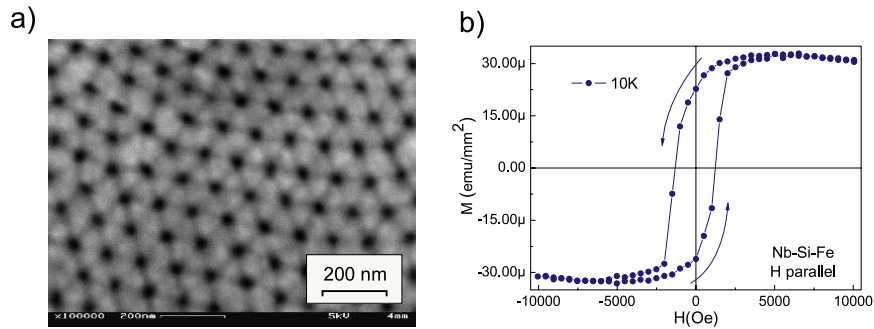


Figure 1. (a) SEM micrograph of the porous Nb film, sample C. (b) $M(H)$ for the sample with magnetic dots, sample B, above T_c , for H applied parallel to the film surface, indicating that the dots are in-plane magnetized.

10%–90% transition width is $\Delta T_c = 0.9$ K determined with the same technique. For a triangular array of strong pinning potentials $d = (100 \pm 10)$ nm apart, the first matching field is $H_M = \frac{2}{\sqrt{3}}(\phi_0/d^2) = (2310 \pm 460)$ Oe.

3. Results and discussion

To identify the state of the magnetic dots in sample B, the normal state magnetization loop, $M(H)$, at $T = 10$ K was determined for the parallel field configuration and is shown in figure 1(b). The observed field dependence clearly indicates that the Fe nanodots are not in magnetic vortex state but in single magnetic domains with in-plane magnetization, suggesting that magnetic reversal takes place via coherent rotation, as expected for their size (further magnetic characterization can be found elsewhere [26, 27, 29]).

The $T_c(H)$ phase boundary was roughly extracted from field cooled $\chi_{ac}(H, T)$ measurements, for the three samples, fitting the data with the expression $H_{c2}(T) = \phi_0/(2\pi\xi^2(T))$ for sample A and $H_{c2}(T) = \sqrt{12}\phi_0/(2\pi\omega\xi(T))$ where ω is the width of the superconducting film between pores or dots [28], yielding the zero temperature coherence lengths $\xi(0) \approx 10, 7$ and 5 nm for samples A, B and C respectively.

Figure 2(a) shows ZFC ac susceptibility (shielding capability) as a function of increasing magnetic field, $\chi'_{ac}(H)$, for sample A (unpatterned Nb film) with open black symbols and for sample B (Nb with Fe dots) with full blue symbols at different temperatures. The samples were cooled in zero magnetic field to the different target reduced temperatures ($t = 0.59, 0.76, 0.83$ and 0.88 for sample A and $t = 0.58, 0.75, 0.83$ and 0.88 for sample B). Different initial protocols were examined, magnetizing or demagnetizing the dots in the normal state before cooling the sample in zero field, but we found no memory of previous normal state magnetic history.

The field dependence of the unpatterned sample follows the behavior of a film in transverse geometry, in the critical state [1], where $\chi'_{ac}(h) \sim \frac{1}{h} \tanh(h)$ with $h = H/H^*(H, T)$ and $H^*(H, T) = \pi J_C(H, T)a$, where J_C is the critical current density and a is the film thickness. However, the field dependence for the patterned film has a strong modulation with a clear decrease in mobility or increase in shielding capability (dip) at $H_M \sim 2000$ Oe for all the measured temperatures. In figure 2(b) we show $\chi'_{ac}(H)$ for sample C (Nb film with

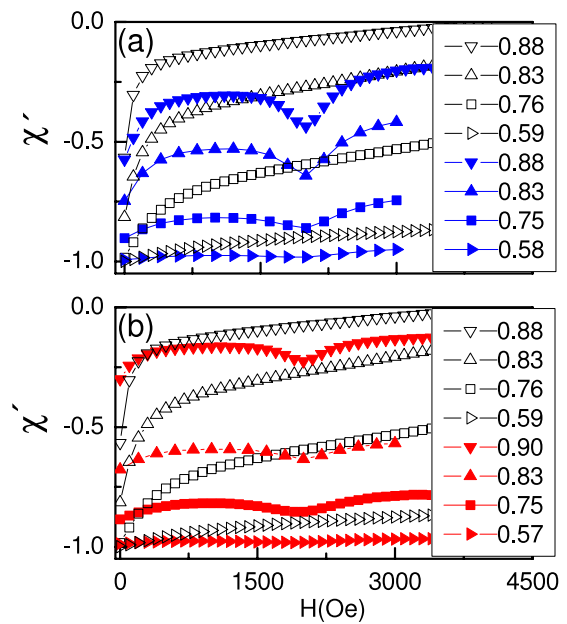


Figure 2. (a) Ac susceptibility χ'_{ac} as a function of increasing field, H , for sample A (Nb film, open black symbols) and sample B (Nb film containing Fe dots, full blue symbols) at different reduced temperatures. (b) χ'_{ac} as a function of increasing field, H , for sample C (Nb film with holes, full red symbols) for different reduced temperatures. The same results for sample A as in panel (a) (open black symbols) are plotted for clarity.

antidots) in full red symbols, for $t = 0.57, 0.75, 0.83$ and 0.90 . We include again (in open black symbols) the same results as shown in figure 2(b) for the unpatterned Nb film (sample A), for comparison. The response of the Nb film with antidots also shows a strong modulation with a decrease in mobility at $H_M \sim 2000$ Oe. In both samples B and C the matching modulation is observed in a wide temperature range, $0.53 < t < 0.95$ (see figures 2 and 3).

A first maximum in mobility occurs for $H \sim H_M/2$. Then the mobility decreases as the field is increased, and reaches a minimum displayed as the dip in $\chi'_{ac}(H)$ for approximately one vortex line per artificial pinning site, close to the geometrical first matching field H_M (we will come back to this below). This result is consistent with simulations of flux-gradient-driven superconducting vortices interacting with triangular arrays

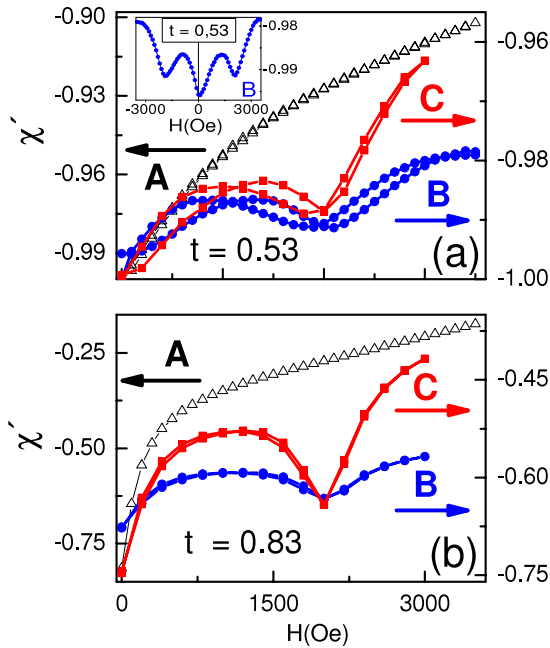


Figure 3. Ac susceptibility $\chi'_{ac}(H)$ for increasing and decreasing positive field for sample A (Nb film, open black triangles), sample B (Nb film containing Fe dots, full red circles) and sample C (Nb film with holes, full blue squares) at (a) $t = 0.53$ and (b) $t = 0.83$. The inset in panel (a) shows $\chi'_{ac}(H)$ for sample B for a field loop at $t = 0.53$ showing symmetry for $\pm H$. See text.

of strong pinning sites in an increasing external magnetic field [30]. In this case a dip in magnetization (local minimum in pinning or local maximum in vortex mobility) is found at approximately $H_M/2$ and a peak in the field dependence of the sample magnetization, $M(H)$ (local maximum in pinning or local minimum in vortex mobility), is found close to H_M (see figure 3(f) in [30]). We note, however, that in these simulations no additional interstitial pinning centers were considered. This is not the case for our samples, where random interstitial pinning sites play a role, as we observe that intrinsic defects in the unpatterned Nb film pin the vortex lattice in sample A leading to high shielding capability at low reduced temperatures. Even though the intrinsic pinning potentials may differ in the different samples, these pinning potentials are known to be present in our Nb films.

We now focus on the irreversibility observed at low temperatures. For clarity, we will show results for positive applied fields. However, the behavior is highly symmetric for negative fields, as illustrated in the inset of figure 3 for sample B. The sample was zero field cooled to $t = 0.53$ and we measured $\chi'_{ac}(H)$ while increasing H to 3000 Oe. Next the magnetic field was reduced to $H = 0$ and $\chi'_{ac}(H)$ was measured as H was decreased to -3000 Oe. These results are in good agreement with in-plane magnetized dots acting as artificial periodic pinning centers [31]. The response for the Nb film with holes (sample C, not shown) is also highly symmetric.

Hysteretic behavior is shown in figure 3(a), where we plot $\chi'_{ac}(H)$ for increasing and decreasing magnetic field for the three samples at the same reduced temperature,

$t = 0.53$. The response for sample A is reversible (open black triangles), while the responses for both patterned samples B (full red circles) and C (full blue squares) are irreversible. With decreasing field, the maximum in mobility shifts to higher fields by almost 350 Oe, and its local minimum, usually assigned to the matching field, also shifts to higher fields, by about 200 Oe. The matching field is expected to have a unique value, which is given by the density of pinning sites in the periodic array; it is the field that induces one flux line per pinning center. However, here we observe that maximum pinning is not uniquely related to commensurability with the periodic potential in samples B and C, as it is history dependent. This behavior cannot be solely produced by the intrinsic interstitial pinning as suggested by the reversible behavior observed for the plain Nb film at the same reduced temperatures. Additionally, the observation of hysteresis in both patterned samples rules out its connection to changes in the magnetic state of the dots induced by the magnetic history.

Another possible explanation for the observed hysteretic behavior is whether there is a significant difference in the magnetic induction B inside the samples in increasing/decreasing branches. In particular, it is expected that B will be lower in the increasing branch than for the stable vortex configuration if surface barriers dominate or larger if demagnetizing effects dominate. To answer this question we performed the field cooling (FC) experiments in sample B shown in figure 4. The zero field cooled (ZFC), increasing branch is plotted in full black squares and the decreasing branch in full red circles. The FC results are shown with full blue triangles, for $t < t^*$ (panel (a)) and $t > t^*$ (panel (b)).

In the FC experiment, the field is applied in the normal state and the sample is cooled to the target temperature. The next point is obtained by warming the sample to the normal state and applying the next field before cooling the sample back to the target temperature to measure $\chi'_{ac}(H)$. In field cooling conditions the vortex lattice configurations are very close to the stable vortex patterns [32]. Demagnetizing effects are reduced, so internal fields approximate applied fields. For $t < t^*$ in panel (a), the vortex lattice response for the ZFC increasing field branch coincides with the response in the FC experiment for $H_a < 1000$ Oe. This coincidence indicates that the magnetic induction B in the sample region where ac penetration occurs is not significantly different from the magnetic induction in the stable vortex pattern, and therefore a difference in B is not the origin of irreversibility. Additionally, in a decreasing branch, B could be expected to be smaller than the applied field, in a similar way to how B is expected to be larger than the applied field as the field is increased [33]; however, both the FC and the ZFC decreasing branch responses coincide down to $H \approx 1500$ Oe.

The reversible behavior of the Nb film for similar low reduced temperatures, having also a high demagnetizing factor, is a further indication that differences in B are not relevant in the increasing and decreasing branches, probably because the very high demagnetizing factors of these samples produce a high penetration of dc fields in the studied field range.

Additionally, the results plotted in panel (b) are consistent with the absence of hysteretic behavior above t^* (see figure 3),

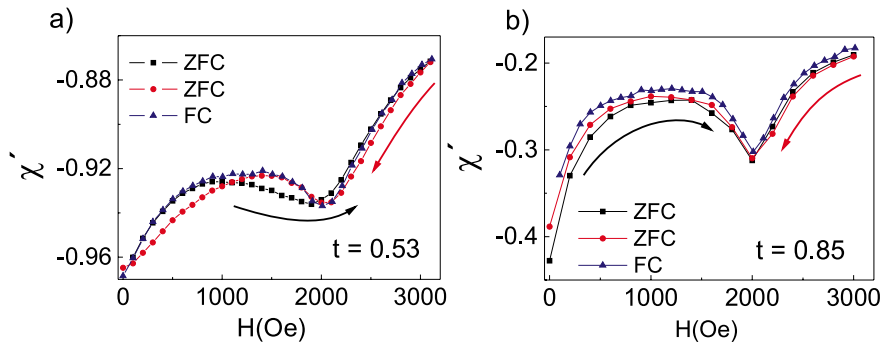


Figure 4. $\chi'_{ac}(H)$ in the ZFC increasing branch (black full squares), the decreasing branch (red full circles) and the FC data (blue full triangles) for the porous sample C: (a) $t = 0.53 < t^*$, (b) $t = 0.83 > t^*$. See text.

and the ZFC increasing/decreasing branches and FC results coincide, consistent with the description that intrinsic pinning is negligible at high temperatures.

It is well known that periodic pinning becomes dominant as compared to random pinning when the temperature is increased. In panel (b) of figure 3, we show $\chi'_{ac}(H)$ for the three samples at a higher reduced temperature, $t = 0.83$. Note that the screening capability has become smaller at $t = 0.83$ than at $t = 0.53$. The depression of the screening capability is more pronounced for sample A, which contains only intrinsic pinning: the susceptibility goes from $-1 < \chi'_{ac}(H) < -0.9$ in panel (a) to $-0.8 < \chi'_{ac}(H) < -0.2$ in panel (b) for the same field range. Note also that, although a strong modulation is observed at the matching fields, the response of samples B and C becomes reversible at $t = 0.83$. This indicates that periodic pinning, which is responsible for matching effects, cannot account by itself for hysteresis. This result also supports the scenario in which the interplay between both random and strong periodic pinning potentials originates the hysteretic behavior.

Having discarded the sources of irreversibility discussed above, we propose below a scenario in which the interplay between random intrinsic and periodic artificial pinning produces metastable VL configurations at low temperatures, and in what follows we address different characteristics of the irreversible behavior in patterned samples.

The gradual loss of hysteretic effects with temperature is illustrated in figure 5, in which we show the response for sample B for selected increasing temperatures, $t = 0.53, 0.57, 0.75$ and 0.83 (panels (a)–(d)), and similar results for sample C ($t = 0.53, 0.58, 0.75$ and 0.83 , panels (e)–(h)). Results for increasing (decreasing) field are plotted in full black (open red) symbols.

The matching field is well defined in ZFC experiments for reduced temperatures above 0.75 in both samples, $H_M = (2000 \pm 100)$ Oe, and coincides with the low temperature matching field in the ZFC decreasing branch (see also figure 3) and the FC matching field value (figure 4). The maximum in mobility becomes also history independent for $t > 0.75$. These results then suggest the existence of a reduced crossover temperature t^* , between 0.75 and 0.83 for both samples, above which metastable VL configurations cannot be sustained.

In order to further examine metastability below t^* , we measured vortex mobility by performing successive field loops. In each loop, the applied dc field H is increased from $H = 0$ to a maximum value, H_{MAX} , and then reduced back to $H = 0$. In the subsequent loop, the field is increased to a higher H_{MAX} before being reduced back to zero. This protocol is repeated in a sequence of loops for increasing maximum field values, identified as H_{MAX}^j , where j indicates the loop number.

Figure 6 shows $\chi'_{ac}(H)$ for sample B (Nb film with Fe nanodot array) at $t = 0.53$ measured for successive magnetic field loops with maximum field $H_{MAX}^j = j \times 500$ Oe ($1 \leq j \leq 8$). For clarity, we have split the sequence of consecutive loops in panels (a)–(d), where increasing (decreasing) branches are plotted with full (open) symbols. The vertical arrows indicate H_{MAX}^j in each panel.

For loops with low H_{MAX} , in particular for $H_{MAX}^1 = 500$ Oe (panel (a)), the behavior is essentially reversible. The hysteresis develops gradually as H_{MAX}^j increases (panels (a)–(d)). Note, however, that the field-increasing branches (full symbols in all panels) coincide in all cases; i.e. the increasing branch in loop j is not affected by the previous $j - 1$ field excursion. This indicates that, after the field is reduced to $H = 0$, there is no trapped flux affecting the vortex dynamics, regardless of the maximum magnetic field attained in the previous loop.

The decreasing field branches exhibit a different behavior between the $\chi'_{ac}(H)$ curves corresponding to loops with $H_{MAX}^j < 2000$ Oe and those corresponding to $H_{MAX}^j > 2000$ Oe. On the one hand, for loops with $H_{MAX}^j < 2000$ Oe (panels (a) and (b)) the field decreasing branches show different mobility depending on the maximum attained magnetic field: we observe that the position of the local maximum in mobility is shifted towards higher field values. On the other hand, for cycles with $H_{MAX}^j > 2000$ Oe (panels (c) and (d)) the field decreasing curves become the same. These results show that the sample attains a unique state after the field is cycled above $H = H_M = 2000$ Oe. This value for H_M is consistent with the calculated first matching field for our samples.

With decreasing temperature the pinning strength of the random defects increases faster than that of the artificial ones. The key point is that, while artificial periodic pinning is on the average stronger than random pinning even at low temperatures

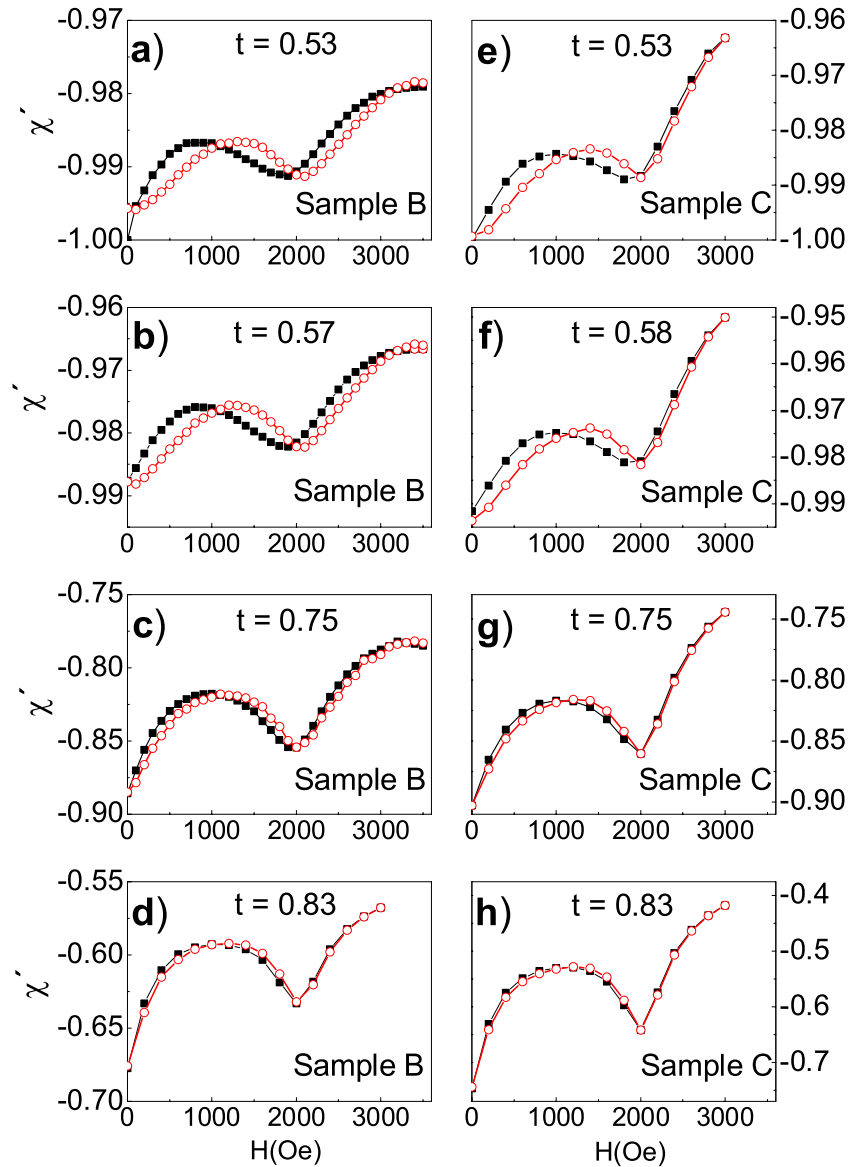


Figure 5. Panels (a)–(d) show ac susceptibility $\chi'_{ac}(H)$ for increasing (full black symbols) and decreasing (open red symbols) field for sample B (Nb film containing Fe dots) for $t = 0.53, 0.57, 0.75$ and 0.83 . Similarly, panels (e)–(h) show results for sample C (Nb film with holes).

(as shown by the presence of commensurability effects), a fraction of the intrinsic pinning sites may individually be as strong as (or stronger than) the artificial ones. Thus, at low temperatures, it may be energetically favorable for a fraction of the vortices to occupy intrinsic pinning sites instead of artificial ones. This will depend on the local energy balance between the pinning and VL elastic energies, as the pinning mode should be mostly of collective nature [7]. The latter, which arises from vortex–vortex interactions, becomes relevant as the applied field is increased.

From the above, a consistent description of the experimental results emerges. For $H_{MAX}^1 \sim H_1/4 = 500$ Oe a large fraction of vortices are in strong pinning sites [30] and few vortices are in interstitial positions showing an almost reversible behavior. The mobility is high because there are plenty of empty sites to be occupied when vortices are forced to

move by ac currents. This high mobility and small hysteresis occurs also for $j = 2$ or $H_{MAX}^2 \sim H_M/2 = 1000$ Oe. As H_{MAX}^j increases, additional vortices start occupying periodic and interstitial pinning sites, accommodating a fraction of the vortices in those intrinsic random defects that provide sufficiently strong pinning. As the vortex–vortex interactions increase with field, these strongly pinned vortices inhibit the motion of other neighboring vortices, that probably become caged [34]. The system needs to overcome a high energy barrier to reorganize; therefore a metastable configuration, that corresponds to a local minimum in the vortex configuration energy landscape, produces a dip in mobility at a value smaller than the first commensurate field. As the amplitude of the applied field increases above the field that induces one vortex per artificial pinning site, $H_M < H$, all the artificial pinning sites become occupied and the rest of the vortices are pinned

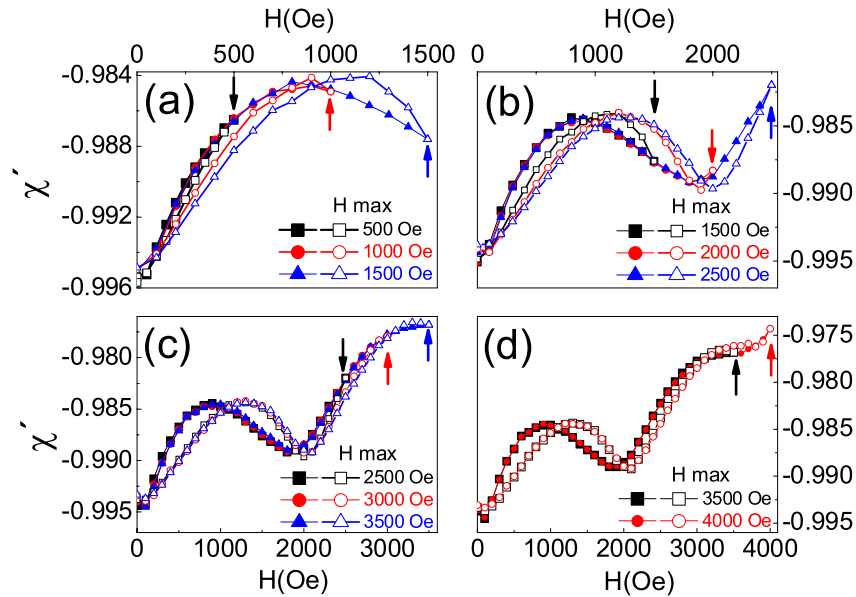


Figure 6. (a) $\chi'_{ac}(H)$ for sample B at $t = 0.53$ for successive magnetic field loops with maximum field $H_{MAX}^j = 500, 1000$ and 1500 Oe; (b) $H_{MAX}^j = 1500, 2000$ and 2500 Oe; (c) $H_{MAX}^j = 2500, 3000$ and 3500 Oe and (d) $H_{MAX}^j = 3500$ and 4000 Oe (see text). The full (open) symbols represent increasing (decreasing) magnetic field. The vertical arrows show H_{MAX}^j in each panel. See text.

in interstitial positions. When the field is reduced, the more weakly pinned interstitial vortices exit the sample first. As we continue reducing the field, either vortices occupying artificial pinning sites or those pinned at the strongest intrinsic sites must exit the sample. Vortices in interstitial positions disturb the ordering of the VL and have a large cost of elastic energy, so these will exit the sample first, even if some of the intrinsic interstitial pinning sites are individually as strong as the artificial ones. When H reaches H_M , all the periodic pinning sites are occupied, independently of the maximum attained field, giving rise to a unique field decreasing branch below H_M . Note that, in our description, before reaching H_M not all the periodic pinning sites are occupied, and interstitial vortices can reorganize in different metastable VL configurations; it is known that the different configurations accessible by the lattice may have different mobilities [35], explaining the various field decreasing branches observed at low dc fields ($j = 2-4$).

As the temperature increases, however, the strength of the intrinsic pinning decreases faster than that of the periodic pinning, the interplay between both pinning sites is lost and the latter dominate, as was shown in figure 5 for $t > t^* \sim 0.75$. Interstitial vortices do not reduce the vortex mobility any longer, and therefore only one VL configuration remains robust at a given field value, i.e. hysteresis becomes negligible. The first matching field is identified with the field for which the number of flux lines equals the number of periodic pinning sites and, consistently, it coincides with the matching field for field decreasing branches or FC experiments.

4. Conclusions

We have studied vortex dynamics in ac susceptibility experiments in Nb films in which intrinsic vortex pinning defects in the films coexist with periodic triangular arrays

of holes or magnetic dots. We have identified matching effects in the vortex mobility related to the periodicity of the artificial pinning centers in a wide temperature range, $0.5 < t < 0.95$, for both types of periodic pinning potentials. Characteristic hysteretic behavior as a function of applied field in ZFC experiments, was found below a crossover reduced temperature, $t^* \sim 0.75$, in both patterned samples. Different experiments were performed to determine which of the possible sources of hysteretic behavior dominates in these samples, and to lead to a consistent description of our observations.

The similarity between the response of both patterned samples discarded the role of magnetic hysteresis of the Fe dots as originating the VL hysteresis. Low temperature FC experiments provided evidence that the hysteresis is not related to different values of the magnetic induction, B , in the ac penetrated region of the samples in the increasing and decreasing field branches. The absence of hysteresis in the response of a plain Nb film supported the previous argument and suggested in addition that this behavior does not originate from a hysteresis produced solely by the random pinning potential. On the other hand, the observation of a crossover temperature above which no hysteretic response is observed in the patterned samples, in coincidence with the strong reduction of the effect of random pinning as temperature is increased while matching anomalies subsist, indicated that the metastable VL configurations are not produced solely by strong artificial pinning. We conclude that our results lead to the consistent picture that the competition between the elastic interaction in the vortex lattice, random and artificial periodic pinning, originates the described behavior, and that these results need to be tested with numerical simulations including both types of competing pinning sources.

Acknowledgments

We thank F Casanova for assistance in Nb deposition and G Jorge for technical assistance. This work was partially supported by UBACyT X13 and CONICET. Work at UCSD supported by US NSF, RTRA ‘Triangle de la Physique’ funding (SUPRASPIN) is acknowledged.

References

- [1] Mikheenko P N and Kuzovlev Yu E 1993 *Physica C* **204** 229
Clem J R and Sanchez A 1994 *Phys. Rev. B* **50** 9355
Brandt E H 1995 *Rep. Prog. Phys.* **58** 1465
Babich I M, Mikitik G P and Brandt E H 2006 *Phys. Rev. B* **74** 224501
- [2] Daldini O, Martinoli P, Olsen J L and Berner G 1974 *Phys. Rev. Lett.* **32** 218
- [3] Fiory A T, Hebard A F and Somekh S 1978 *Appl. Phys. Lett.* **32** 73
- [4] Pruyboom A, Kes P H, van der Drift E and Radelaar S 1988 *Phys. Rev. Lett.* **60** 1430
- [5] Otani Y, Pannetier B, Nozières J P and Givord D 1993 *J. Magn. Magn. Mater.* **126** 22
- [6] Martín J I, Vélez M, Nogués J and Schuller Ivan K 1997 *Phys. Rev. Lett.* **79** 1929
Van Bael M J, Temst K, Moshchalkov V V and Bruynseraede Y 1999 *Phys. Rev. B* **59** 14674
Van Bael M J, Bekaert J, Temst K, Van Look L, Moshchalkov V V, Bruynseraede Y, Howells G D, Grigorenko A N, Bending S J and Borghs G 2001 *Phys. Rev. Lett.* **86** 155
Montero M I, Akerman J J, Varilci A and Schuller Ivan K 2003 *Europhys. Lett.* **63** 118
Villegas J E, Savel’ev S, Nori F, González E M, Anguita J V, García R and Vicent J L 2003 *Science* **302** 1188
Lange M, Van Bael M J and Moshchalkov V V 2005 *J. Low Temp. Phys.* **139** 195
Lyuksyutov I F and Pokrovsky V L 2005 *Adv. Phys.* **54** 67
Silhanek A V, Gillijns W, Moshchalkov V V, Metlushko V and Ilic B 2006 *Appl. Phys. Lett.* **89** 182505
- [7] Villegas J E, Montero M I, Li C-P and Schuller Ivan K 2006 *Phys. Rev. Lett.* **97** 027002
- [8] Kemmler M *et al* 2006 *Phys. Rev. Lett.* **97** 147003
- [9] Rosen Y J, Sharoni A and Schuller Ivan K 2010 *Phys. Rev. B* **82** 014509
- [10] Martín J I, Vélez M, Hoffmann A, Schuller Ivan K and Vicent J L 1999 *Phys. Rev. Lett.* **83** 1022
- [11] Vélez M, Martín J I, Villegas J E, Hoffmann A, González E M, Vicent J L and Schuller Ivan K 2008 *J. Magn. Magn. Mater.* **320** 2547
- [12] Aladyshkin A Yu, Silhanek A V, Gillijns W and Moshchalkov V V 2009 *Supercond. Sci. Technol.* **22** 053001
- [13] Hoffmann A, Prieto P and Schuller Ivan K 2000 *Phys. Rev. B* **61** 6958
- [14] Raedts S, Silhanek A V, Van Bael M J and Moshchalkov V V 2004 *Phys. Rev. B* **70** 024509
- [15] Baert M, Metlushko V V, Jonckheere R, Moshchalkov V V and Bruynseraede Y 1995 *Phys. Rev. Lett.* **74** 3269
- [16] Jaccard Y, Martin J I, Cyrille M-C, Velez M, Vicent J L and Schuller Ivan K 1998 *Phys. Rev. B* **58** 8232
- [17] Grigorenko A N, Bending S J, Van Bael M J, Lange M, Moshchalkov V V, Fangohr H and de Groot P A J 2003 *Phys. Rev. Lett.* **90** 237001
Kramer R B G, Silhanek A V, Van de Vondel J, Raes B and Moshchalkov V V 2009 *Phys. Rev. Lett.* **103** 067007
- [18] Villegas J E, Gonzalez E M, Sefrioui Z, Santamaría J and Vicent J L 2005 *Phys. Rev. B* **72** 174512
- [19] Martin J I, Vélez M, Nogues J and Schuller Ivan K 1997 *Phys. Rev. Lett.* **79** 1929
Metlushko V V *et al* 1999 *Phys. Rev. B* **60** R12 585
Terentiev A, Watkins D B, De Long L E, Morgan D J and Ketterson J B 1999 *Physica C* **324** 1
Terentiev A, Watkins D B, De Long L E, Cooley L D, Morgan D J and Ketterson J B 2000 *Phys. Rev. B* **61** R9249
- [20] Welp U, Xiao Z L, Jiang J S, Vlasko-Vlasov V K, Bader S D, Crabtree G W, Liang J, Chik H and Xu J M 2002 *Phys. Rev. B* **66** 212507
- [21] Eming T and Nattermann T 1997 *Phys. Rev. Lett.* **79** 5090
Dong Noh J and Rieger H 2001 *Phys. Rev. Lett.* **87** 176102
Pogosov W V, Mismo V R, Zhao H J and Peters F M 2009 *Phys. Rev. B* **79** 014504
- [22] Patel U, Xiao Z L, Hua J, Xu T, Rosenmann D, Novosad V, Pearson J, Welp U, Kwok W K and Crabtree G W 2007 *Phys. Rev. B* **76** 020508R
- [23] Reichhardt C and Olson C J 2002 *Phys. Rev. Lett.* **88** 248301
Reichhardt C and Olson C J 2004 *Phys. Rev. Lett.* **92** 108301
- [24] Le Doussal P and Giamarchi T 1998 *Phys. Rev. B* **57** 11356
- [25] Civale L, Worthington T K, Krusin-Elbaum L and Holtzberg F 1992 *Magnetic Susceptibility of Superconductors and Other Spin Systems* ed R A Hein, T L Francavilla and D H Liebenberg (New York: Plenum) p 313
Coffey M W and Clem J R 1992 *Phys. Rev. B* **45** 9872
van der Beek C J, Geshkenbein V B and Vinokur V M 1993 *Phys. Rev. B* **48** 3393
- [26] Li C-P, Roshchin I V, Battle X, Viret M, Ott F and Schuller Ivan K 2006 *J. Appl. Phys.* **100** 074318
- [27] Villegas J E, Li C-P and Schuller Ivan K 2007 *Phys. Rev. Lett.* **99** 227001
- [28] Tinkham M 1975 *Introduction to Superconductivity* (New York: McGraw-Hill)
- [29] Villegas J E, Sharoni A, Li C P and Schuller Ivan K 2009 *Appl. Phys. Lett.* **94** 252507
- [30] Reichhardt C, Groth J, Olson C J, Field Stuart B and Nori F 1997 *Phys. Rev. B* **54** 16108
- [31] Hoffmann A, Fumagalli L, Jahedi N, Sautner J C, Pearson J E, Mihajlović G and Metlushko V 2008 *Phys. Rev. B* **77** 060506R
- [32] Clem J R and Hao Z 1993 *Phys. Rev. B* **48** 1377
- [33] Clem J R and Sánchez A 1994 *Phys. Rev. B* **50** 9355
- [34] de Souza Silva Clécio C, Albino Aguiar J and Moshchalkov V V 2003 *Phys. Rev. B* **68** 134512
- [35] Pasquini G, Pérez Daroca D, Chliotte C, Lozano G S and Bekeris V 2008 *Phys. Rev. Lett.* **100** 247003